

# Nano-Optical Studies of Superconducting Nanowire Single Photon Detectors

John A.O'Connor<sup>1</sup>, Paul A. Dalgarno<sup>1</sup>, Michael G. Tanner<sup>1</sup>, Richard J. Warburton<sup>1</sup>, Robert H. Hadfield<sup>1</sup>, Burm Baek<sup>2</sup>, Sae Woo Nam<sup>2</sup>, Shigehito Miki<sup>3</sup>, Zhen Wang<sup>3</sup>, and Masahide Sasaki<sup>3</sup>

<sup>1</sup> Heriot Watt University, Edinburgh, United Kingdom

<sup>2</sup> National Institute of Standards and Technology (NIST), Boulder, Colorado, USA

<sup>3</sup> National Institute of Information and Communications Technology (NICT), Japan  
jao10@hw.ac.uk

**Abstract.** Single-photon detectors based upon superconducting nanowires offer single-photon sensitivity from the visible well into the infrared, encompassing the crucial telecommunication wavelengths. In addition they benefit from low dark counts (Hz) and low timing jitter (sub 100 ps). These detectors have recently been employed in photon-counting applications such as quantum cryptography and characterization of quantum emitters. Key challenges in the development of this emerging single-photon detector technology are improving device uniformity and improving optical coupling efficiency. We report on photoresponse mapping of superconducting nanowire single-photon detectors using nano-optical techniques. The device is mounted on a high resolution translation stage and illuminated with a focal spot significantly smaller than the device area (20  $\mu\text{m}$  x 20  $\mu\text{m}$ ). Using a confocal microscope configuration, we achieve a diffraction limited spot size of 800 nm at  $\lambda = 950$  nm. We have previously shown that uniform (high detection efficiency) and constricted (low efficiency) nanowire devices give contrasting photoresponse signatures – a broad plateau response across the whole device and a single point response respectively. Recent work on purposely-designed low fill-factor devices (100 nm linewidth, 1  $\mu\text{m}$  period) has allowed us to resolve individual 100 nm width wires.

**Keywords:** Superconducting nanowire single photon detectors, SSPD, SNSPD.

## 1 Introduction

Advances in optics and nanotechnology allow the interaction between light and matter to be studied on ever decreasing length scales which may hold the key to gaining insights into fundamental physics and developing new technologies. The use of nano-optical techniques [namely confocal microscopy in conjunction with high refractive index solid immersion lens (SIL)] allows us to focus light with sub-micrometre precision onto nanostructured superconducting wires and to map their photoresponse[1].

Superconducting nanowire single-photon detectors (SNSPDs) based on superconducting nanowires hold great promise as a new type of high-speed, high sensitivity single-photon detector, with a spectral range from the visible well into the infrared. The basic device concept was pioneered by Gol'tsman *et al.*[2]. A 100 nm wide wire is patterned by electron beam lithography and reactive ion etching in an ultrathin

(~4 nm thick) NbN superconducting film. The superconducting wire (operated in the temperature range 1.5–5 K) is biased close to its critical current  $I_C$ . An incident visible or infrared photon perturbs the current distribution, triggering a fast voltage pulse with picosecond rise time. The largest area nanowire SSPDs now available[3] consist of a meander wire (100 nm linewidth, 200 nm period) covering an area up to  $20 \times 20 \mu\text{m}^2$ , compatible with a single mode telecommunications fibre. SSPDs have been successfully employed in quantum information processing applications, spanning quantum cryptography[4,5], quantum emitter characterization[6-10], and quantum logic circuits[11].

## 2 Photoresponse Mapping

Figure 1 shows the mapping setup. This apparatus provides a platform for excellent optical and spatial resolution, by combining a confocal microscope (using aspheric

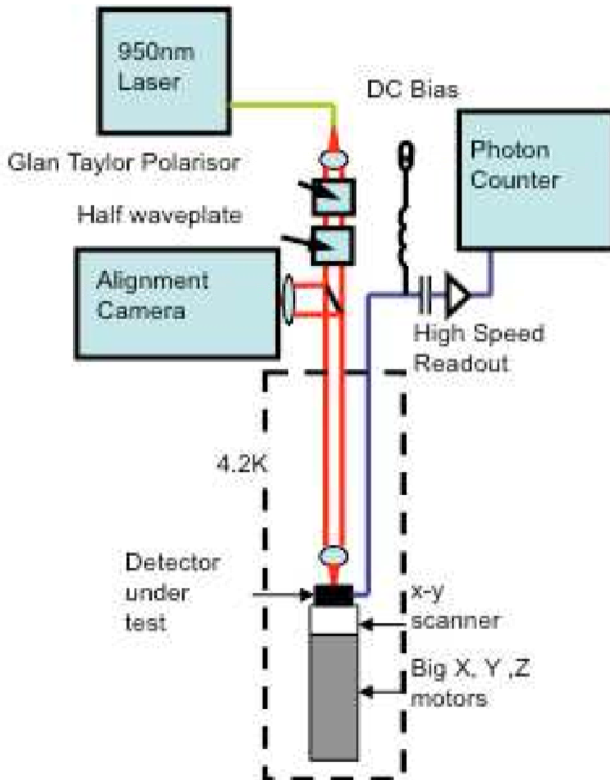


**Fig. 1.** Photoresponse mapping setup. This configuration affords high resolution scanning over a  $30 \times 30 \mu\text{m}^2$  area. The confocal microscope has a short working distance and high NA. The sample is mounted on low temperature piezoelectric linear positioners. The device is electrically connected for biasing and readout of photodetection events. A Glan Taylor polarizer is used to define the state of linear polarisation and the half waveplate is used to rotate the linear polarisation state (0-360°).

lenses) with XYZ piezoelectric linear positioners at 4.2K. The camera aids optical alignment. The sample space is filled with He vapour and is immersed in liquid He.

The resolution limit by Sparrow's criterion[12] is

$$FWHM = \frac{0.52\lambda}{NA} \quad (1)$$

Where FWHM is the full width at half maximum of the focal spot,  $\lambda$  is the wavelength,  $NA$  is the numerical aperture of the objective lens. The resolution can be boosted further (by a factor of the refractive index  $n$ ) via use of a hemispherical solid immersion lens[1,13].

In this study, the devices tested were both  $20 \times 20 \mu\text{m}^2$  area[3], but of differing fill factors: 10% (100 nm linewidth, 1  $\mu\text{m}$  period) and 50% (100 nm linewidth, 200 nm period).

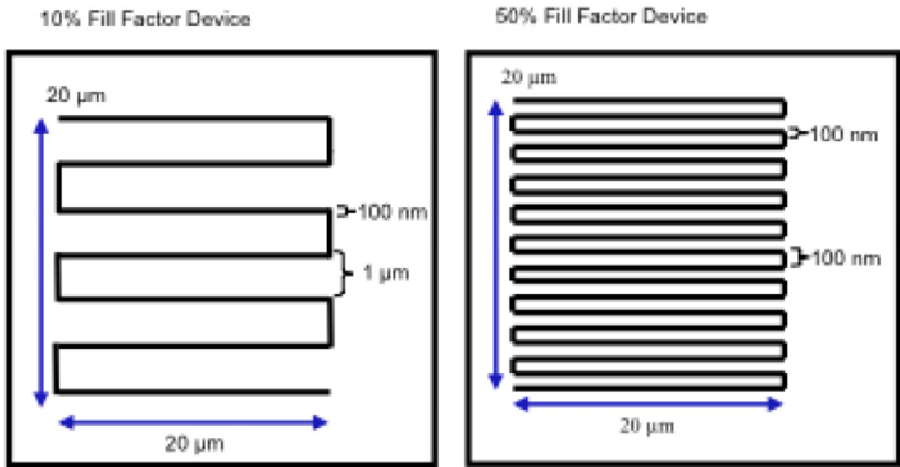


**Fig. 2.** Schematic of 10% and 50% fill factor devices

The 10% device was mounted in the confocal microscope. Using an objective lens with  $NA=0.68$ , the device was mapped using a continuous wave (cw) laser at  $\lambda=950$  nm and a pulsed laser at  $\lambda=975$  nm. Qualitatively the same response was seen at both wavelengths. Figure 3(A) shows that the individual wires in the device have been resolved. The one thing that is noticeable is that there is a missing line in the device that is electrically connected but is not photosensitive to the same extent as the rest of the device; this is due to that section of the wire having a lower current density than across the rest of the device. Possibly this is due to this wire being wider or thicker than the rest of the device.

The 50% device was mounted and mapped in the same way as the 10% device. Figure 3(B) shows a reasonably uniform response indicated by the plateau, which

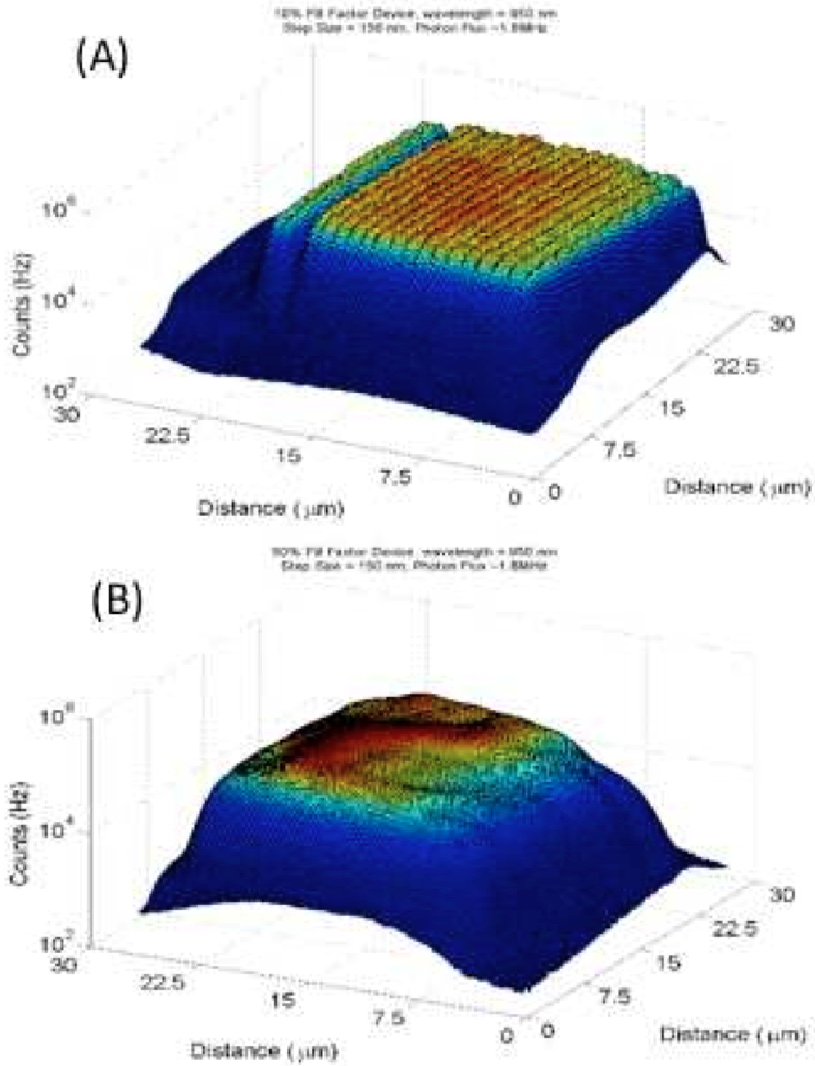


**Fig. 3.** Photoresponse maps, photon flux  $\sim 2$  MHz, device area  $20 \mu\text{m} \times 20 \mu\text{m}$ ,  $\lambda=950 \text{ nm}$ , FWHM spot size  $800 \text{ nm}$ . (A) 10% device (100 nm linewidth,  $1 \mu\text{m}$  period) with wires distinguishable. (B) 50% device (100 nm linewidth,  $200 \text{ nm}$  period) with uniform photoresponse.

varies by no more than a factor of 2. Again at both wavelengths qualitatively the same response was seen. For these measurements the background count rate was  $\sim 200$  Hz and the photon flux was  $\sim 2$  MHz.



Kinetic inductance is observed to increase as the critical current is approached[17] due to the increased current density. This increase is less in a device with constrictions as the current density in the majority of the device is still far from the critical current density. Through fitting with a suitable model the limiting constriction in the device can be characterised, in this  $C = 0.654$  and  $C = 0.376$  for the 10% and 50% fill factor devices respectively, where  $C$  is the ratio of the constriction cross sectional area to the unconstructed superconducting cross section of the wire. As the value for the

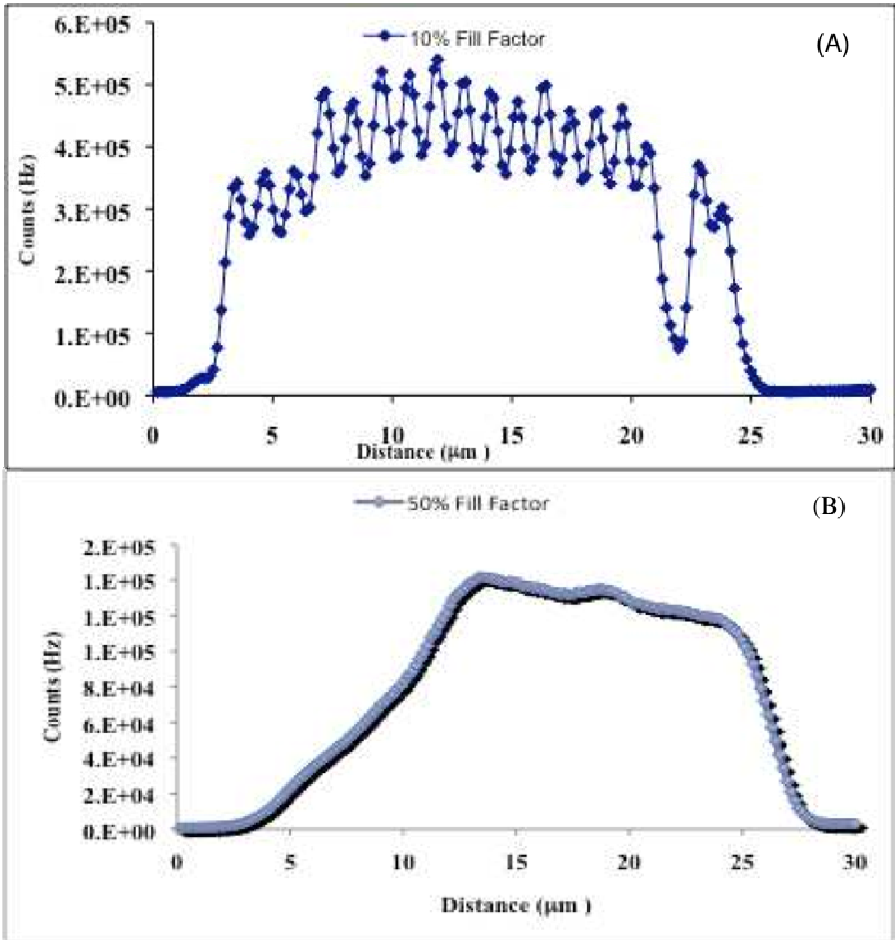


**Fig. 4.** (A) 10% Fill Factor device line scan perpendicular to the wires of the device. Missing line (still electrically connected) is visible. (B) 50% Fill Factor device line scan perpendicular to the wires. One edge is well defined and the other is less so depicted by the smaller gradient slope.

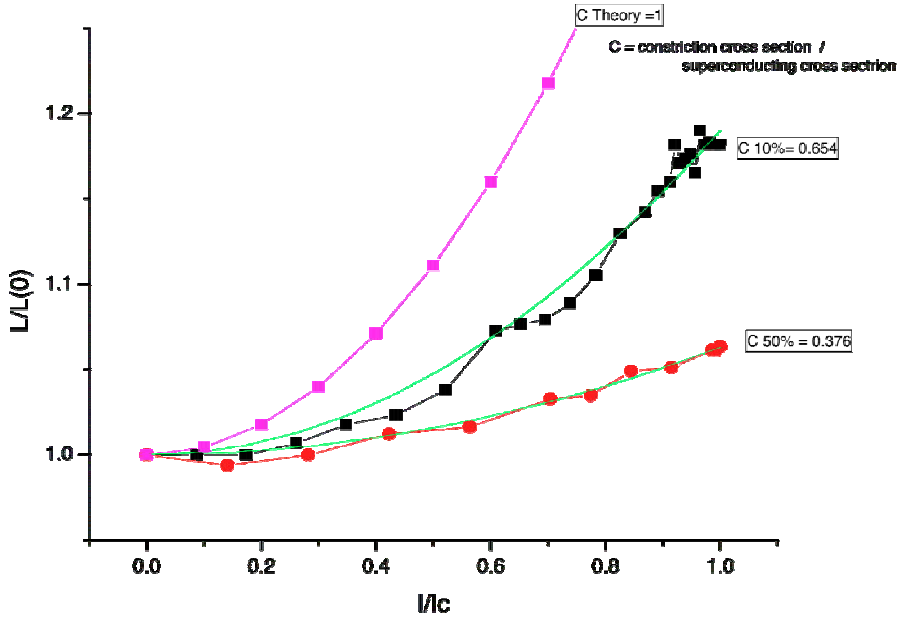


**Fig. 5.** Inductance trend approaching critical current (black squares for 10% fill factor and red circles for 50% fill factor devices) with fit from theory (green lines) and reference fit of unconstructed device (magenta squares).

10% device is close to 1 the whole length of the nanowire is able to approach the critical current achieving the high uniformity observed. The high value of  $C$  again suggests good fabrication was achieved. While conversely the lower value of  $C$  for the 50% device indicates a possible constriction in the nanowire suggesting the uniformity of the fabrication is not as good as the 10% device.

### 3 Polarisation Dependence

The linear polarisation state of the light that is incident on the device can affect the performance and efficiency of the devices. Polarisation effects of the devices have been shown and reported before[14-16]. We measured this effect in on both 10% and 50% fill factor devices.

The results show that polarisation dependence of both devices gives a maximum count rate with the light polarised parallel to the wires and a minimum count rate with the light polarised perpendicular to the wires. This agrees with theoretical models of absorption that have been carried out and reported by Anant et al[16].

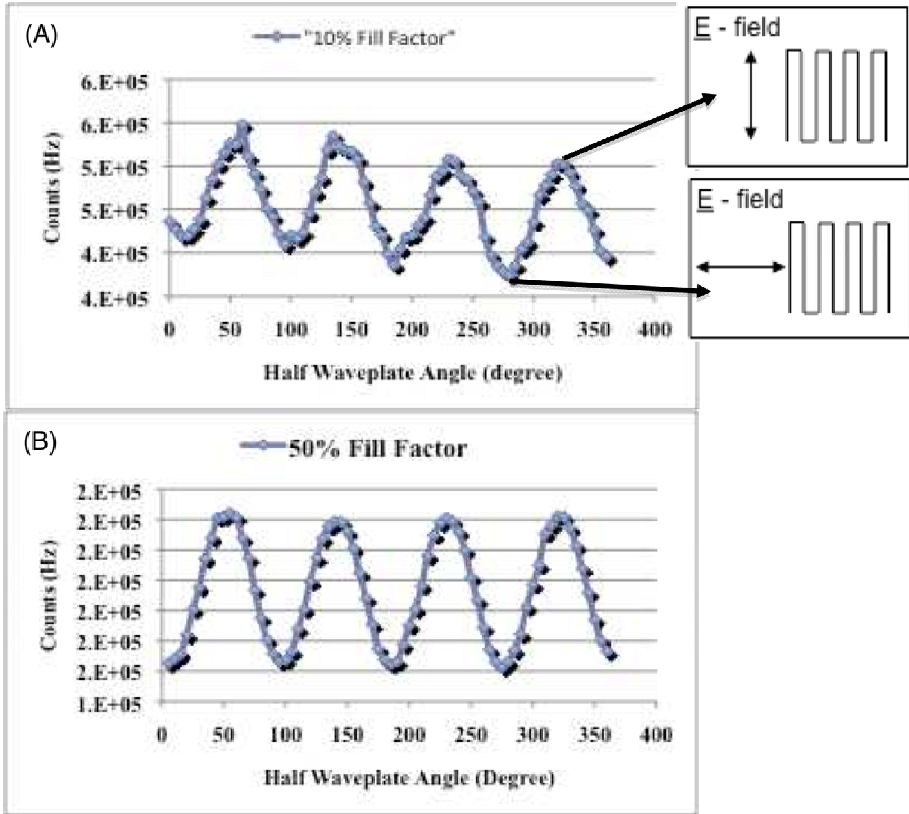


**Fig. 6.** Results of polarisation dependence for (A) 10% fill factor device and, (B) 50% device illuminated by 950nm laser light. Where  $50^\circ$  (and repeats every  $90^\circ$ ) aligns the polarisation of the light to be parallel to the wires of the device, and  $95^\circ$  (and repeating every  $90^\circ$ ) is aligned perpendicular to the wires.

## 4 Conclusion and Outlook

We have successfully carried out photoresponse mapping studies with submicrometer precision using a confocal microscope configuration. In recent experiments we have made complete photoresponse maps of 10% and 50% fill factor devices and are able to resolve individual wires in the former case. Both the 10% and 50% fill factor devices show polarisation dependences which varies in extent with the wavelength of the incident light. We plan to extend these studies to investigate local variations in timing jitter. Furthermore this enhanced optical coupling will allow us to study and explore novel device designs (e.g. nanoantennae) which may prove to be easier than the meander design to fabricate with higher quantum efficiencies, allowing scaling up to multi-pixel devices.

## Acknowledgements

JAO, PAD, RJW, RHH thank the UK EPSRC for support. RHH is also supported by a Royal Society of London University Research Fellowship.

## References

1. Hadfield, R.H., Dalgarno, P.A., O'Connor, J.A., Ramsay, E., Warburton, R.J., Gansen, E.J., Baek, B., Stevens, M.J., Mirin, R.P., Nam, S.: Submicrometer photoresponse mapping of nanowire superconducting single-photon detectors. *Appl. Phys. Lett.* 91, 241108 (2007)
2. Gol'tsman, G.N., Okunev, O., Chulkova, G., Lipatov, A., Semenov, A., Smirnov, K., Voronov, B., Dzardanov, A., Williams, C., Sobolewski, R.: Picosecond superconducting single-photon optical detector. *Appl. Phys. Lett.* 79, 705 (2001)
3. Miki, S., Fujiwara, M., Sasaki, M., Baek, B., Miller, A.J., Hadfield, R.H., Nam, S., Wang, Z.: Large sensitive-area NbN nanowire superconducting single-photon detectors fabricated on single-crystal MgO substrates. *Appl. Phys. Lett.* 92, 061116 (2008)
4. Hadfield, R.H., Habif, J.L., Schlafer, J., Schwall, R.E., Nam, S.: Quantum key distribution at 1550 nm with twin superconducting single-photon detectors. *Appl. Phys. Lett.* 89, 241129 (2006)
5. Takesue, H., Nam, S., Zhang, Q., Hadfield, R.H., Honjo, T., Tamaki, K., Yamamoto, Y.: Quantum key distribution over a 40-dB channel loss using superconducting single-photon detectors. *Nat. Photonics* 1, 343 (2007)
6. Hadfield, R.H., Stevens, M.J., Gruber, S.S., Miller, A.J., Schwall, R.E., Mirin, R.P., Nam, S.: Single photon source characterization with a superconducting single photon detector. *Opt. Express* 13, 10846 (2005)
7. Stevens, M.J., Hadfield, R.H., Schwall, R.E., Nam, S., Mirin, R.P., Gupta, J.A.: Fast lifetime measurements of infrared emitters using a low-jitter superconducting single-photon detector. *Appl. Phys. Lett.* 89, 031109 (2006)
8. Liang, C., Lee, K.F., Medic, M., Kumar, P., Hadfield, R.H., Kumar, P.: Characterization of fiber-generated entangled photon pairs with superconducting single-photon detectors. *Opt. Express* 15, 1322 (2007)
9. Hadfield, R.H., Stevens, M.J., Nam, S., Mirin, R.P.: Single-photon source characterization with twin infrared-sensitive superconducting single-photo detectors. *J. Appl. Phys.* 101, 103104 (2007)
10. Zinoni, C., Alloing, B., Li, L.H., Marsili, F., Fiore, A., Lungi, L., Gerardino, A., Vakhromin, Y.B., Smirnov, K.V., Gol'tsman, G.N.: Single-photon experiments at telecommunication wavelengths using nanowire superconducting detectors. *Appl. Phys. Lett.* 91, 031106 (2007)
11. Chen, J., Altepeter, J.B., Medic, M., Lee, K.F., Gokden, B., Hadfield, R.H., Nam, S., Kumar, P.: Demonstration of a quantum controlled-NOT gate in the telecommunications band. *PRL* 100, 133603 (2008)
12. Sparrow, C.M.: On spectroscopic resolving power. *Astrophys. J.* 44, 76 (1916)
13. Serrels, K.A., Ramsay, E., Dalgarno, P.A., Gerardot, B., O'Connor, J.A., Hadfield, R.H., Warburton, R.J., Reid, D.T.: Solid immersion lens applications for nanophotonic devices. *J. Nanophotonics* 2, 021854 (2008)

14. Driessen, E.F.C., Braakman, F.R., Reiger, E.M., Dorenbos, S.N., Zwiller, V., de Dood, M.J.A.: Polarization measurements on NbN SNSPDs 480 nm – 1550 nm. *Eur. Phys. J. Appl. Phys.* 47, 10701 (2009)
15. Dorenbos, S.N., Reiger, E.M., Akopian, N., Perinetti, U., Zwiller, V., Zijlstra, T., Klapwijk, T.M.: Superconducting single photon detectors with minimized polarization dependence. *APL* 93, 161102 (2008)
16. Anant, V., Kerman, A.J., Dauler, E.A., Yang, J.K.W., Rosfjord, K.M., Berggren, K.K.: Optical properties of superconducting nanowire single-photon detectors. *Opt. Express* 16, 10750 (2008)
17. Kerman, A.J., Dauler, E.A., Keicher, W.E., Yang, J.K.W., Berggren, K.K., Gol'tsman, G.N., Voronov, B.: Kinetic-inductance-limited reset time of superconducting nanowire photon counters. *Appl. Phys. Lett.* 88, 111116 (2006)